Supplementary Materials For:

Rapid exocytosis kinetics measured by amperometry within volcano microelectrodes

Nicolas Grégoire Maïno*, Arnaud Bertsch*, Philippe Renaud

Microsystems Laboratory 4, École Polytechnique Fédérale de Lausanne (EPFL), 1015 Lausanne, Switzerland

* nicolas.maino@epfl.ch , arnaud.bertsch@epfl.ch

TABLE OF CONTENT:

LIST OF FIGURES:

Section 1: Fabrication of the volcano microelectrodes /nanogap device

The fabrication process flow is depicted step by step in the supplementary materials (Supp. Figure 1). Before starting the process, the FS substrates are cleaned in two consecutive piranha baths (three part sulfuric acid 97% one part 30% hydrogen peroxide) for 5 mn each followed by thorough rinsing in two consecutive ultra-pure deionized water (DIW) bath before spin-drying. In step A) a stack of thin metal layers consisting of Ti/Au/Cr with thickness 7/50/70 nm is evaporated using an EVA760 (Alliance Concept, France) e-beam evaporator. In step B) The sacrificial chromium layer is patterned into disks of 100 µm of diameter with bean-shaped openings that will define the SiO_2 pillars. This is achieved by spin-coating the substrate with a 600nm thick AZ ECI 3007 i-line photoresist (MicroChemicals, Germany) with an ACS Gen 3 automated spin-coater (Süss MicroTec, Germany). The desired pattern is then exposed using a MA6GEN3 mask aligner (Süss MicroTec, Germany) in i-line mode (365 nm) with a dose of 165 mJ/cm^2 and developed with the same automated coater starting with a 60 s post-exposure bake with a proximity of 100 µm to a hotplate set to 110°C , cooling down for 15 s on a cool plate and subsequent development in AZ MIF726 developer with a total contact time of 27 s. Before etching the resist is reflown by direct contact with a Sawatec HP200 hot plate (Sawatec, Switzerland) set to 125°C for 60 s. This step together with the use of a thin photoresist layer and a tilt of the stage during the next etching step is critical to prevent fence formation along the pattern by redeposition of the etched material during ion beam etching. Chromium is then etched using Ar^+ ion bombardment using a IBE350 (Veeco, USA) set to 300 V acceleration voltage, 500 mA beam current and with a stage tilt with respect to the incident beam of -30°. The etching is monitored using an integrated secondary ions mass spectrometer (SIMS) and stopped 5 s after the appearance of the Au signal. The photoresist is then partially removed by carefully subjecting the substrate to a short oxygen plasma etching of 100 W with an oxygen flow of 400 mL/min for 1 mn using a TePla 300 microwave plasma system. Without initial dry etching, the photoresist layer is unremovable using wet resist stripping alone. This is because the top layer of photoresist has become hardened from ion implantation during Ar^+ ions bombardment in the previous step. This hardening effect is proportional to ion beam acceleration voltage, beam current and total etching time hence the use of a moderate acceleration voltage above. Short time of oxygen plasma etching with moderate power did not result in etching of the chromium underneath as evidenced by features dimension unaffected within the resolution afforded by optical microscopy. Finally the bulk of the photoresist layer is removed by immersion in two consecutive baths of 70°C Remover 1165 (Dow Chemical Company, USA) for 5 mn each before rinsing in two consecutive DIW baths and spin-drying. In the following steps C), E) and G) the same workflow for photolithography and etching is used with the same machine and materials (i.e. Az ECI 3007). Accordingly, in step C) the underlying Au electrode, leads and contact pads are defined by photolithography, etching and careful resist removal as described above. In step D) a 200 nm layer of SiO_2 is deposited by PECVD, see supplementary figure 2 for detailed deposition parameters, on an Oxford plasmalab system 100 (Oxford Instruments, UK). In step E), the SiO_2 layer is patterned to open the contact area to the chromium layer. In this step the bean-shaped openings in the chromium layer that were filled by SiO_2 in the previous step are protected from etching by the photoresist mask thereby creating the SiO_2 pillars. In step F) a stack of thin metal layers consisting of Cr/Au/Ti with thickness 5/60/7 nm is sputtered using a DP650 (Alliance Concept, France). The use of sputtering over evaporation is to ensure good step coverage of the underlying SiO_2 pattern. In step G) the metal stack is patterned as in step C) and E). At this point the resistivity from one electrode's contact pad to the second forming the electrode pair can be measured

to verify the good inter-layer contact and was between 3 and 4 kohm with our design. In step H) a second layer of SiO_2 of 300 nm thickness is deposited by PECVD as described above. In step I) the VMEs are defined as described previously.[1] A 1.6 µm thick layer of AznLoF2020 photoresist (MicroChemicals, Germany) is spin coated and 2.25 µm diameter openings are defined by exposure with a VPG200 direct laser writer (Heidelberg, Germany) with a 355 nm UV light dose of 13 mJ/cm^2. To obtain photoresist straight wall, the manufacturer exposure dose recommendation for an 1.6 µm thick layer of AznLoF2020 is 80 mJ/cm^2 but we found that optimal values to obtain the desired pattern lateral dimension were significantly different on glass substrate as well as dependent on the pattern dimension. Thereby the exposure dose used in this step should be optimized on a substrate/design basis. The post-exposure bake is conducted at 110°C with 100 µm proximity gap for 75 s followed by 51 s contact time development with AZ MIF726. In this step the photoresist reflow is omitted and substrates are immediately subjected to ion beam etching as described above but with 500 V beam acceleration voltage, 800 mA beam current and 0° incidence angle. Etching is stopped 1mn10 after the appearance of the chromium signal or as soon as the Au signal arising from the bottom electrode etching appears. Photoresist is removed as described above. SEM images were acquired using a Merlin SEM (Zeiss, Germany) with an extraction voltage of 1.5 kV and a beam current of 30 pA and a secondary-electron detector. The wafers were diced on a DAD321 (Disco, Germany) with a resinoid blade of 70 µm width under 25 000 rpm rotation moving at 1 mm/s from the top side of the wafer. A glass O-ring was glued on top of the individual chips using PDMS and cured overnight at 60°C in a convection oven.

Section 2: Device preparation

Individual devices were cleaned with a 3 min oxygen plasma (100 W, 650 mTorr; Diener Electronic, Germany) followed by immediate filling of the culture chamber with pure ethanol to ensure proper wetting of the inside of the VMEs. The culture chamber content was then exchanged with DIW 6 times and chromium wet etchant 2 times (TechniEtch Cr01, MicroChemicals, USA). The etching of the chromium layer was accelerated as described by others.[2] All 28 VMEs of the device were connected together to the working electrode of an Stat.h bipotentiostat (Ivium, The Netherlands). The counter electrode used was a platinum wire and the reference electrode was a saturated Mercurous/Mercurous sulfate electrode (OGR011; Origalys, France). The working electrodes were biased by +150 mV with respect to the open circuit potential and the current and charge passed was monitored for 2 min (Supp. Figure 3). Completion of the chromium etching was assessed by the charge passed reaching a plateau (1.33 mC for our design). From this point onward, the culture chamber was never dried and any liquid exchange was performed by leaving a small amount to ensure the device would not dry which could result in sticking of the electrodes pair due to surface tension (not tested).The culture chamber content was exchanged 6 times with DIW and 2 times with a solution of KCl 250 mM and the device yield was assessed at this point by biasing both electrodes of a given volcano microelectrode (VME) to different potentials (e.g. 0 mV top electrode and +500 mV bottom electrode) and counting out the VME whose electrodes were shorted as evidenced by current overload.

Section 3: Electrochemical characterization of the gold electrodes

For characterization purposes devices after chromium etching were filled with an aqueous solution of 1 mM ferrocenemethanol (335061, Merck) and 250 mM KCl. Both electrodes of the VME were connected together and used as a working electrode controlled by a Stat.h bipotentiostat (Ivium, The Netherlands) together with a platinum wire and KCl saturated reference silver/silver chloride electrode (MF-2056; BaSi, USA) serving as counter and reference electrode respectively. Cyclic voltammograms between +100 mV and +400 mV were acquired at a scan rate of 2 mV/s and the average of the last three cycles were taken. The cyclic voltammogram (Supp. Figure 4, A) shows a current trace close to a sigmoid curve as is expected for microelectrodes scanned at low scan rate reaching close to 100 pA.[3] Amperometric traces were acquired in the same solution by stepping the VME electrodes potential from 0 to +600 mV and sampling the current every 10 ms. The background-subtracted steady-state current obtained is about 100 pA (Supp. Figure 4, B-C).

Section 4: Quantification of catecholamine content in PC12 cells

To ascertain the catecholaminergic nature of the electroactive molecules found in the PC12 cells we used in this study, we used a fluorometric measurement following the reaction of catecholamine with 3-hydroxyphenyl boronic acid.[5] This assay is selective to dopamine although we did not include a control for norepinephrine so we refer to the electroactive molecules measured from PC12 cells exocytosis throughout this study as catecholamines collectively.

PC12 cultures were washed twice in ice-cold PBS and collected by pipette dislodgement from their substrate. The number of cells was assessed by counting on an automated hemocytometer (TC20™; Bio-Rad, USA) after trypan blue staining. The cell suspension was centrifuged at 2000 g for 2 mn. The supernatant was discarded and the cells resuspended in 100 µL PBS to which we added 100 µL of trichloroacetic acid (TCA) at 0.5 M and sonication at room temperature for 10 mn. The TCA was neutralized by addition of 22.8 µL of KOH 2M and the resulting solution was serial diluted to obtain three samples diluted according to a semi-log scale. The three diluted samples per culture were pipetted into a 94-well plate for reader plate together with concentration standards of dopamine used as calibration. All culture and calibration samples were then mixed with 160 µL of 25 mM Na_2CO_3 (pH = 10.5) and 200 µL of 8 mM 3-hydroxyphenyl boronic acid and imaged after 10 mn incubation at room temperature protected from light. Samples were excited at 417 nm and fluorescence measured at 464 nm with a bandpass of 10nm on both filters. The optimal gain was assessed on the calibration samples of highest concentration and kept constant throughout all readings. The calibrations yielded the following regression equation: concentration (µM) = 0.0244 x F/F0 + 1.71 where F is the fluorescence intensity at 464 nm and F0 is the background fluorescence of a blank sample. The determination coefficient R^2 was equal to 0.996.

The mean catecholamine content of the PC12 cells was 1.5 ± 0.22 femtomol **(**Supp. Figure 6, n=2 cultures), which is in agreement with previous published measurements.[6] Cultures incubated with Levodopa before lysis had a 2-fold higher amount of catecholamine with 3.36 ± 0.44 femtomol per cell (n=2 cultures) in agreement with report of increased quantal size after levodopa incubation.[7]

Section 5: Comparison of the new electrochemical nanogap fabrication process

The fabrication of the device is exceptionally robust considering the pair of electrodes in each VME are separated by 75 nm only in the nanogap region. The yield obtained is consistently above 85% which is a marked improvement to the 50% achieved before for nanogap of 40 nm.[8] Although in our implementation the nanogap's vertical dimension is almost twice as large, the robustness of our fabrication methods allowed us to build nanogaps with electrode overlap of 7000 μm^2. This is over ten times larger than other nanogaps presented in the scientific literature.[8,9] Still it should be pointed out that since microelectrode noise in amperometric measurements scales with the electrode surface area,[10] our implementation is adapted to physiological concentration range but would be unable to achieve single-molecule electrochemical detection as was achieved with nanogap by others.[8]

Our fabrication process is largely independent on residual stress in the different layers thanks to the silicon dioxide (SiO_2) pillars that ensure that the electrodes remain separated after removal of the chromium layer. A strategy used by others to prevent sticking of the electrodes within nanogaps focused on balancing the stress of the thin dielectric films deposited, notably by alternating layers of compressive SiO_2 and tensile silicon nitride (Si_3N_4) deposited by PECVD.[8] This elegant approach however suffers from an irremediable drawback when working with glass substrates. Under the same deposition conditions, Si_3N_4 deposited on silicon and fused silica substrates by PECVD have respectively large tensile and compressive residual stress. The origin of this difference stems from different epitaxial growth depending on the substrate as evidenced by stress measurements after depositions on different substrates (Supp. Figure 2). Our design incorporating SiO_2 pillars between the electrodes is hence a work-around for this issue that has the merit of being applicable to any geometry and allows one to vary the thickness/material of the electrodes and dielectric layer without having to match stresses between layers.

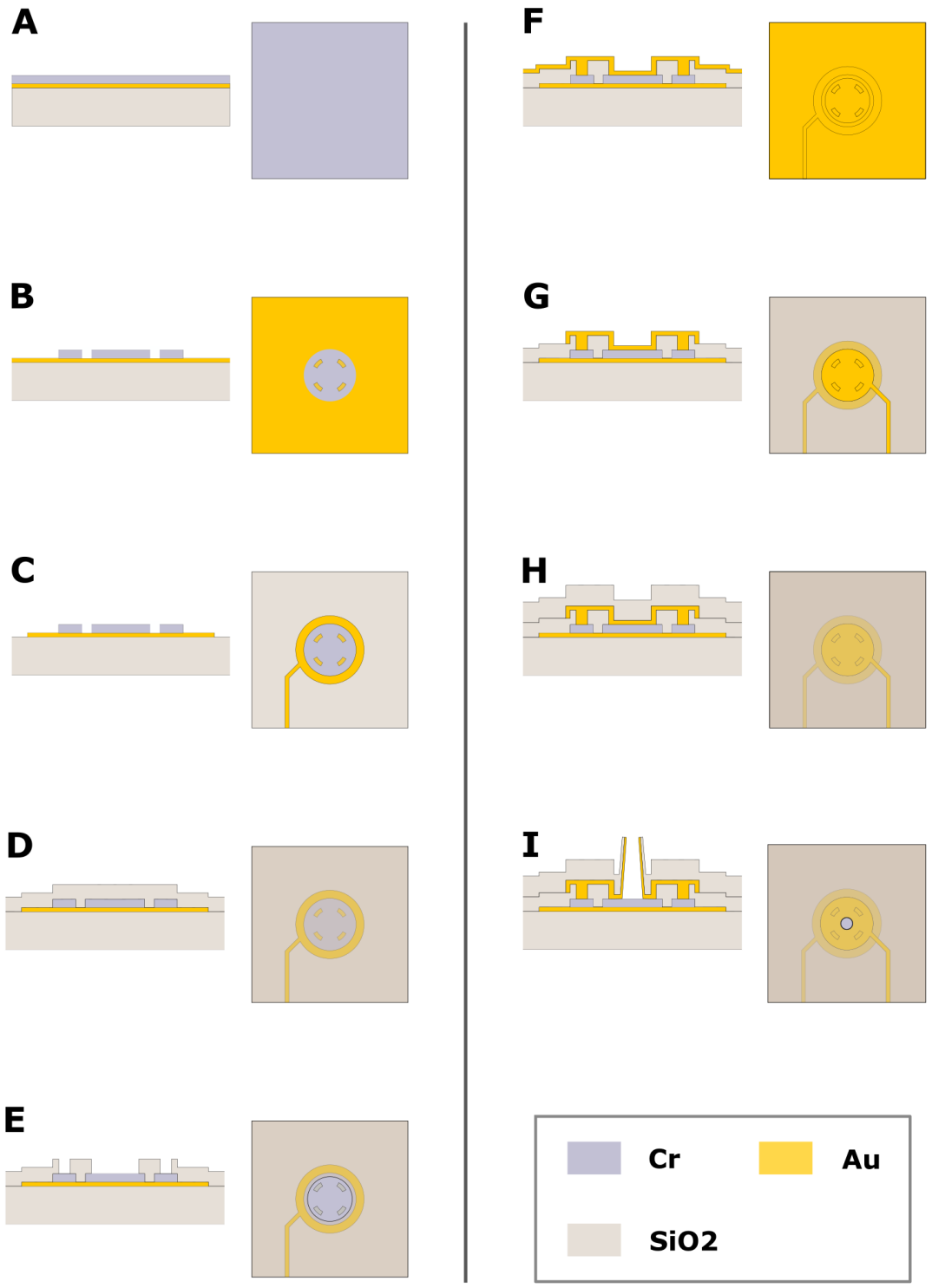

Supp. Figure 1 Volcano microelectrode (VME) fabrication process flow. See Materials and Methods for detailed description (A) Metal evaporation, (B) sacrificial chromium layer patterning, (C) bottom electrode, lead and contact pad patterning, (D) plasma enhanced chemical vapor deposition (PECVD) of silicon dioxide, (E) patterning of the silicon dioxide, (F) top electrode metal sputtering, (G) top electrode, lead and pad patterning, (H) second PECVD of silicon dioxide and (I) patterning of VMEs and access holes to contact pads.

Wafer N°	Substrate	Machine	Material deposited	Temp. (C)	Time (mn,s)	Thickness (nm)*	SiH4/N2 (sccm)	N2O (sccm)	NH3 (sccm)	Pressure (mTorr)	RF power (W)	measured stress 0° (MPa)**	measured stress 90° (MPa)**
	Silicon												
WSi25	Si test	Oxford Instrument Plasmalab System (PECVD)	SiO	300	1mn40	100	400	710	0	1000	20	-301.62	-377.15
WSi23	Si test	Oxford Instrument Plasmalab System 100	SiN	300	6mn27	200	1000	0	15	800	40	192.85	207.12
WSiWOX1	Si test + 500nm Wet Oxide	Oxford Instrument Plasmalab System 100	SiO	300	1mn40	100	400	700	0	1000	20	-272.1	-319.91
WSiWOX2	Si test + 500nm Wet Oxide	Oxford Instrument Plasmalab System 100	SiN	300	3mn20	100	1000	0	15	800	40	206.45	211.62
				* Thickness from theoretical deposition rate, not m									
				** Measurement: Wafer bend (Stoney equation), Machine: Toho FLX-2320-S Wafers were rotated to have main flat facing South (0°) or West (90°) to obtain two measurements									
	Glass												
WFS17SiO	Fused Silica	Oxford Instrument Plasmalab System 100	SiO	300	3mn20	200	400	710	0	1000	20	-621.38	-618
WFS15SiN	Fused Silica	Oxford Instrument Plasmalab System 100	SiN	300	6mn27	200	1000	0	15	800	40	-229.88	-230.82

Supp. Figure 2. Stress measurement of silicon dioxide and silicon nitride deposited by PECVD on different substrates as assessed by wafer bow. Despite equal deposition parameters the resulting residual stresses are markedly different between silicon substrate (with or without oxide) and fused silica substrate which arise from different epitaxial growth. Silicon nitride is often used in conjunction with silicon dioxide to obtain stress free membranes by alternating layers of each material.The measurements reported here show that this approach is however not possible on fused silica substrate as silicon nitride has a large compressive stress.

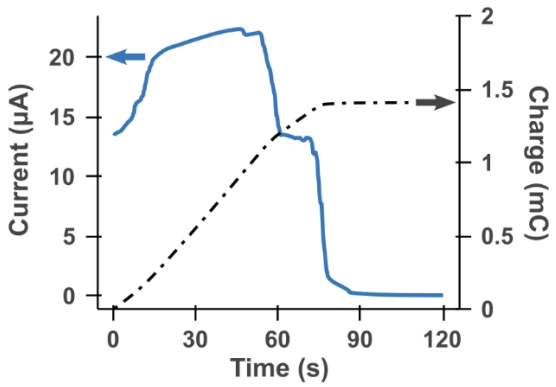

Supp. Figure 3. Sacrificial chromium layer removal by potential assisted wet etching. The graph displays the current passed (left y-axis) and total charge (right y-axis) monitored over the whole etching process lasting 2 mn for a device. The current is seen to decrease abruptly at 60 s and a second time at 85 s since this design of chip housed two versions of the device: one with silicon dioxide pillars and one without (14 devices of each design). Completion of the chromium etching is visible from current dropping below tens of nanoamps and the charge passed reaching a plateau (1.33 mC in this case).

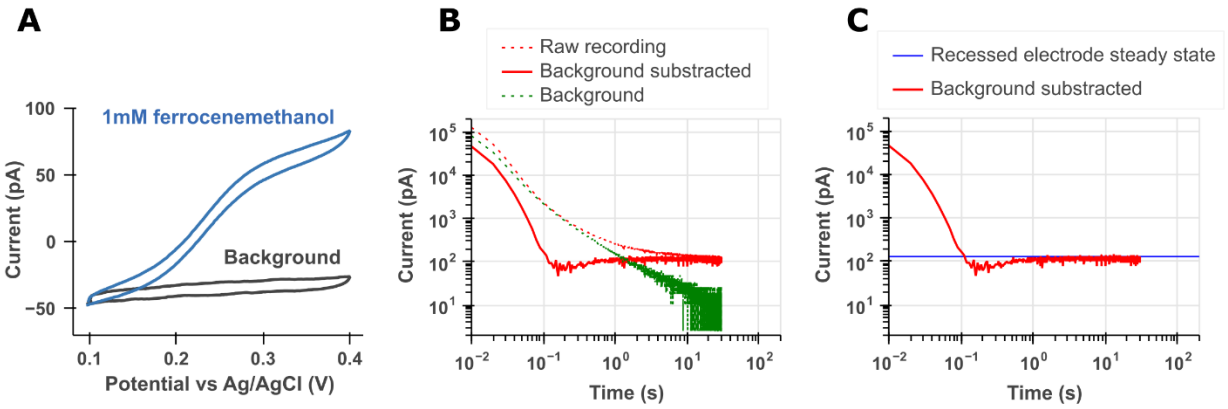

Supp. Figure 4. Cyclic voltammogram and step amperometry from a volcano microelectrode (VME) in an aqueous solution of 250 mM KCl without (Background) or with (Raw) 1 mM ferrocenemethanol. The two electrodes of a given VME were connected together and their potential stepped to +600 mV. (A) Cyclic voltammogram obtained from a single VME in an aqueous solution of 1 mM ferrocenemethanol and 250 mM KCl showing a sigmoid shape typical of microelectrodes. (B) Background, raw and background-subtracted current traces. (C) Comparison of the background subtracted trace to the theoretical steady-state current of a recessed microelectrode[4] of 3.14 μm^2 positioned at the bottom of a recess of depth 0.5 μm. The VME operated in step amperometry reaches a steady state value within 100 milliseconds. Note that this does not represent the time constant of the VME when measuring exocytotic packet as the settling time of the electrode toward steady state at 100 milliseconds probably arises from depletion of the nanocavity from the ferrocenemethanol molecules. The VME is not strictly speaking a recessed electrode because of its conductive inner wall. Sill the comparison to the recessed electrode model suggests that most molecules diffusing inside the VME (towards the electrode) during a potential controlled experiment are consumed within half a micron after entering the VME.

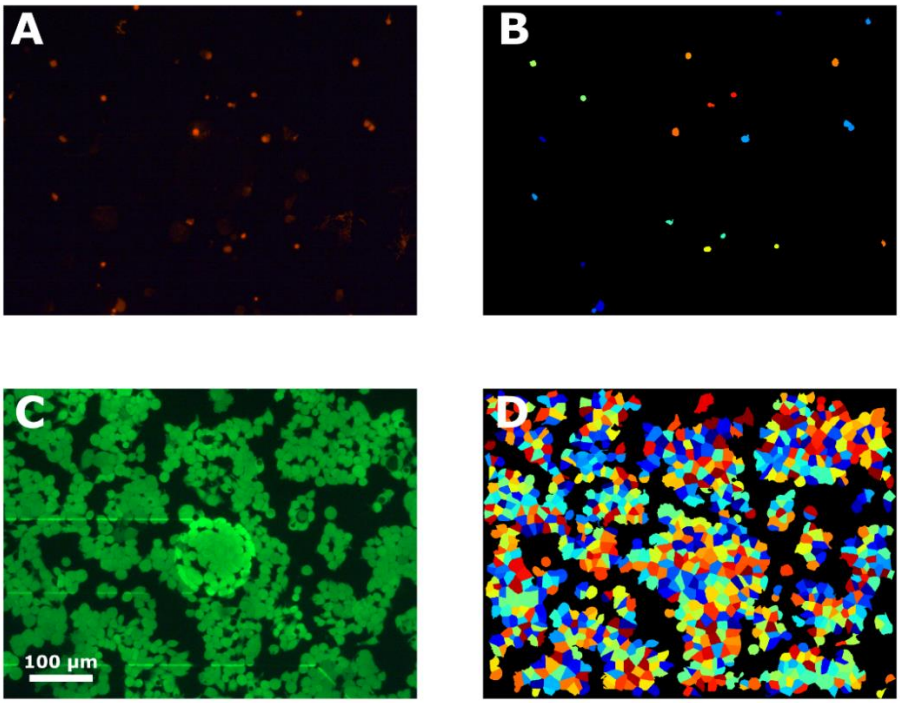

Supp. Figure 5. Live and dead human embryonic kidney cells revealed by calcein-AM and ethidium homodimer-1 staining respectively. (A) and (C) correspond to epifluorescence images of the dead and live stain respectively. (B) and (D) are the output of the CellProfiler pipeline used to identify, segment and count the dead and live cells respectively. Region of increased background fluorescence in (C) corresponds to electrode and electrical leads.

A

Expectation (Greene and Rein 1977)		
moles per cell [moles]	Cell number	Total catecholamine [moles]
5.00E-15	1.00E+06	5.00E-09

B

	This study		
Well label	moles per cell [moles]	Cell number	Total catecholamine [moles]
A1	1.73E-15	1.67E+06	2.89E-09
A2	1.27E-15	1.69E+06	2.16E-09
average	**1.50E-15**	**1.68E+06**	**2.52E-09**
B1 (LD 1h30)	3.80E-15	1.89E+06	7.18E-09
B2 (LD 1h30)	2.92E-15	1.68E+06	4.90E-09
average	**3.36E-15**	**1.78E+06**	**6.04E-09**

Supp. Figure 6. Result of the catecholamine quantification from PC12 cell cultures using a 3-hydroxyphenyl boronic acid fluorometric assay. Cells were lysed with or without pre-treatment with levodopa for 1h30 which is known to increase the total pool of catecholamine in PC12 cells. (A) Previous result of catecholamine quantification in PC12 cultures. (B) Results from catecholamine from PC12 cultures with or without levodopa pre-treatment. The result is in agreement with (A). As expected levodopa increased the catecholamine content per cell.

References

1 B. X. E. Desbiolles, A. Bertsch and P. Renaud, Ion beam etching redeposition for 3D multimaterial nanostructure manufacturing, *Microsyst. Nanoeng.*, 2019, **5**, 1–8.
2 W. Sparreboom, J. C. T. Eijkel, J. Bomer and A. van den Berg, Rapid sacrificial layer etching for the fabrication of nanochannels with integrated metal electrodes, *Lab. Chip*, 2008, **8**, 402–407.
3 R. G. Compton and C. E. Banks, *Understanding Voltammetry: Simulation of electrode processess (Third Edition)*, World Scientific, 2018.
4 A. M. Bond, D. Luscombe, K. B. Oldham and C. G. Zoski, A comparison of the chronoamperometric response at inlaid and recessed disc microelectrodes, *J. Electroanal. Chem. Interfacial Electrochem.*, 1988, **249**, 1–14.
5 X. Liu, M. Tian, W. Gao and J. Zhao, A Simple, Rapid, Fluorometric Assay for Dopamine by In Situ Reaction of Boronic Acids and cis-Diol, *J. Anal. Methods Chem.*, 2019, **2019**, e6540397.
6 L. A. Greene and G. Rein, Release, storage and uptake of catecholamines by a clonal cell line of nerve growth factor (NGF) responsive pheochromocytoma cells, *Brain Res.*, 1977, **129**, 247–263.
7 E. Pothos, M. Desmond and D. Sulzer, l-3,4-Dihydroxyphenylalanine Increases the Quantal Size of Exocytotic Dopamine Release In Vitro, *J. Neurochem.*, 1996, **66**, 629–636.
8 S. Kang, A. F. Nieuwenhuis, K. Mathwig, D. Mampallil and S. G. Lemay, Electrochemical Single-Molecule Detection in Aqueous Solution Using Self-Aligned Nanogap Transducers, *ACS Nano*, 2013, **7**, 10931–10937.
9 E. Kätelhön, B. Hofmann, S. G. Lemay, M. A. G. Zevenbergen, A. Offenhäusser and B. Wolfrum, Nanocavity Redox Cycling Sensors for the Detection of Dopamine Fluctuations in Microfluidic Gradients, *Anal. Chem.*, 2010, **82**, 8502–8509.
10 J. Yao and K. D. Gillis, Quantification of noise sources for amperometric measurement of quantal exocytosis using microelectrodes, *Analyst*, 2012, **137**, 2674–2681.